JOURNAL OF AIRCRAFT
Vol. 34, No. 2, March–April 1997

Airfoil Design for Helicopter Rotor Blades—A Three-Dimensional Approach

Ahmed A. Hassan* and Bruce D. Charles*
McDonnell Douglas Helicopter Systems, Mesa, Arizona 85205

A finite difference procedure has been developed for the design of airfoil sections for helicopter rotor blades. The procedure is based on the coupled three-dimensional direct solutions to the full potential equation inherent in the rotor flow solver (RFS2) and the two-dimensional inverse solutions to an auxiliary equation. Here, the evolution of the airfoil geometries, at a number of a priori defined radial control stations is driven by the user-prescribed pressure distributions and the flowfield requirements imposed by the RFS2 flow solver. In this respect, the influence of the finite aspect ratio blade, sweep, taper and, more importantly, the tip vortex wake, are reflected in the final airfoil designs. The lifting-line CAMRAD/JA trim code was incorporated into the design procedure to allow for the simulation of the tip vortex wake effects. Results are presented for the redesign of a number of airfoil sections for a generic hovering rotor (with rectangular blades) with and without allowance for the tip vortex wake effects. Aerodynamic performance characteristics of the original blade and the redesigned blade in hover are assessed using the three-dimensional TURNS Navier–Stokes rotor flow solver.

Introduction

TRADITIONALLY, there are four basic steps in the sizing of a helicopter rotor blade that meets certain target aerodynamic requirements. These steps are 1) selection of the tip speed to provide for an efficient hovering rotor while maintaining good balance between autorotation characteristics and low noise levels; 2) selection of the rotor diameter to provide for an acceptable disc loading; 3) selection of the rotor solidity that is driven by the maximum figure of merit as well as maneuver capability; and 4) deciding on the appropriate combination of twist and taper (amount and radial position) to maintain, as practicable, a uniform induced velocity distribution over the blade without degradation in autorotation capability. Once the global geometric features of the rotor are established, a more detailed phase of the design is initiated.

In this phase, based on the performance goals of the rotor, airfoil sectional aerodynamic characteristics such as lift and moment coefficients are defined at a number of a priori selected radial stations along the blade. For example, on the advancing portion of the rotor disk, airfoils located near the tip of the blade must exhibit low drag characteristics at low to moderate angles of attack and transonic Mach numbers. On the other hand, on the retreating portion of the rotor disk, airfoils with high-lift capability at low to moderate Mach numbers are required. Low sectional pitching moments are also required to minimize control loads. The question then arises as to what airfoil geometries are required to meet the set aerodynamic performance goals (e.g., rotor thrust, figure of merit, etc.). To address this question, airfoil designers have relied, for many years, on personal experience and on the use of cut and try simple linear analysis methods. More recently, these methods were expanded to include the application of two-dimensional nonlinear computational methods that can be broadly classified as direct iterative methods and inverse design methods.

In direct iterative methods, solutions are sought with an airfoil shape that is modified in an iterative procedure to minimize the differences between the computed and the target aerodynamic characteristics (e.g., lift and/or drag coefficients). Examples of these design methods are those of Hicks and Vanderplaats[1] and Davis.[2] On the other hand, in inverse methods,[3–7] an airfoil geometry is sought that will exhibit certain desirable properties for the flow past the section (e.g., delay of transition or separation of the boundary layer). These conditions are usually met by imposing certain constraints on the velocity distribution along the surface. The ability to design rotor blades that will provide a given velocity or pressure distribution is therefore highly desirable. Moreover, at high blade tip speeds, local regions of supersonic flow occur and shock waves are likely to form with the attendant wave drag and shock-induced boundary-layer separation losses. A shock-free flow would, of course, be desirable as it avoids these losses.

Today, with the advent of high-speed supercomputers and the improvement in the efficiency of three-dimensional rotor flow solvers, we can accurately predict the salient aerodynamic features of a given rotor design. These solvers, however, if considered in conjunction with simple two-dimensional design techniques, can provide a comprehensive design tool that can be used to efficiently provide the detailed three-dimensional geometric description of the blade, exclusive of taper and sweep. For example, one can design a rectangular blade that exhibits the same radial aerodynamic characteristics that are normally achieved with the combined effects of taper and sweep. With a rectangular blade, however, manufacturing costs are lower, the loads problems associated with twist are reduced, and the signature problems inherent with leading-edge sweep are avoided. For rotorcraft, not only will this new class of design tools account for the actual three-dimensional nature of the flow on the blade, but they will also allow for the inclusion of the far wake effects that, to this date, have been overlooked by designers using traditional two-dimensional airfoil design methods. From a practical point of view, the new design tool should be robust to allow for its application over a wide range of operating conditions and, more importantly, it should also provide accurate results at a reasonable cost. Among present-day three-dimensional unsteady rotor flow solvers, those based on the full potential equation (with or without an integral boundary-layer formulation) represent prime candidates for this comprehensive design methodology.

Presented as Paper 90-1588 at the AIAA 21st Fluid Dynamics, Plastic Dynamics, and Lasers Conference, Seattle, WA, June 18–20, 1990; received April 11, 1994; revision received Dec. 18, 1996; accepted for publication Dec. 18, 1996.

*Engineering Specialist, Flight Technology. Member AIAA.

Similar methods have been widely used in the fixed wing industry to design three-dimensional wings.[8,9]

In this paper we describe an engineering method for the design of a helicopter rotor blade having a prescribed pressure, or lift, distribution. The design method is based on the coupling between the three-dimensional full potential rotor flow solver (RFS2)[10] and an extension[11] of the inverse two-dimensional iterative residual correction formulation by Garabedian and McFadden.[12] In this formulation, an auxiliary equation based on the classical wavy wall equations[13] for subsonic and supersonic flows is solved iteratively. In the design method, the auxiliary equation is used to relate the changes in the predicted three-dimensional blade surface pressures at the user-specified control stations to the changes in the local airfoil geometry. In this respect, the evolution of the final blade geometry (only as regards the definition of the various airfoil sections) is driven by the three-dimensional solution that takes into account the finite aspect ratio of the blade and any taper and sweep effects that may have been, a priori, stipulated by the design team.

To account for the far-wake effects, we have taken advantage of the fact that the wake structure remains the same for two different blades that have identical radial lift distributions. In the present design procedure, the lifting-line helicopter/rotor trim code CAMRAD/JA[14] was used to compute the rotor trim state as well as the far-wake-induced angles of attack. To demonstrate the applicability of the procedure, the problem for the hovering rotor will only be considered here. Results with and without the inclusion of the far-wake-induced effects are presented. Conclusions relating to the efficiency of the design method, its limitations, and its accuracy are made.

Mathematical Models

Three-Dimensional Full Potential Rotor Flow Solver RFS2

As mentioned earlier, the three-dimensional solutions for the flow past the rotor were obtained using the RFS2 flow solver developed by Sankar and Prichard.[10] In this section, the equation governing the flow and boundary conditions are briefly described.

The governing equation expressing conservation of mass for a three-dimensional, compressible, unsteady, inviscid flow in an arbitrary curvilinear coordinate system, ξ, η, ζ, τ, is given by

$$(\rho/Ja^2)[\phi_{\tau\tau} + U\phi_{\xi\tau} + V\phi_{\eta\tau} + W\phi_{\zeta\tau}] = [(\rho U/J)_\xi + (\rho V/J)_\eta + (\rho W/J)_\zeta] + S \quad (1)$$

where the ξ direction is aligned with the blade chordwise direction x; the η direction with the spanwise or radial direction y; the ζ direction roughly with the normal direction to the blade z; J is the Jacobian of the coordinate transformation; U, V, and W are the contravariant velocity components; and S is a function that contains terms related to the motion of the grid. Refer to Ref. 10 for the details of the numerical solution algorithm.

In the present study, a three-dimensional rigid grid (attached to the blade in the rotating blade-fixed coordinate system) was constructed by the interpolation of two-dimensional near-orthogonal sheared parabolic C-type grids generated at user-selected blade radial stations (see Fig. 1). The two-dimensional grids were constructed using Jameson's[15] algebraic grid generation procedure built into the RFS2 flow solver.

Numerical Boundary Conditions

Referring to Fig. 1 we notice that the present formulation requires boundary conditions to be specified along the blade's surface, trailing-edge vortex sheet (commonly referred to as near wake or branch cut), far-field boundaries located outboard of the rotor tip, outer boundary, downstream or outflow boundary beyond the blade's trailing edge, and the most inboard

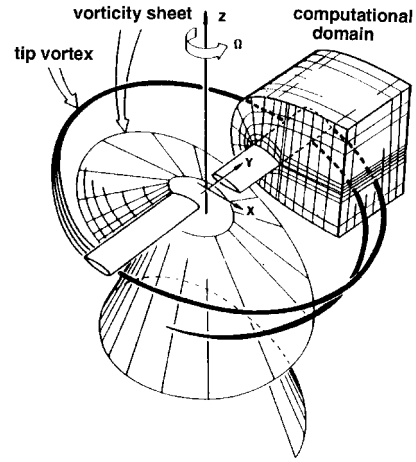

Fig. 1 Sketch of the rotor blade, the computational domain, and the wake system.

boundary of the computational region. For lifting conditions, the effects of the far wake (the portion of the wake that lies outside the bounds of the computational domain) must also be accounted for and modeled in the full potential solution. These boundary conditions are briefly described in the following paragraphs.

Far-field boundaries (outer, downstream, spanwise outboard): Since air is considered to be at rest at a large distance from the blade, the velocity potential function ϕ was set to zero on all three boundaries. This condition also implies that the flow velocities in the planes containing these boundaries assume freestream values. For example, for the spanwise outboard boundary constituting the last computational plane normal to the plane containing the rotor blade, the u and w velocity components were set to zero, whereas the v component, approximately normal to this boundary, was allowed to assume nonzero values. Moreover, at the outer boundary, u and v were set to zero, while w, again approximately normal to this boundary, was allowed to vary. The nonzero normal velocity components, in a sense, allowed waves to propagate through these boundaries. As a result, contamination of the computational domain solutions that may otherwise occur because of far-field wave reflections, was avoided. At the downstream boundary, whenever the local flow was supersonic, a two-point extrapolation formula was used to compute the potential using the interior grid points solutions.

Inboard boundary: This boundary was located at the 55% radial position where ϕ was solved for as part of the numerical solution subject to the following condition:

$$(\rho V/J)_{j=2} = 0 \quad \text{or equivalently} \quad (\phi_\eta)_{j=2} = 0$$

Blade surface: On the solid surface, a slip boundary condition was enforced during the computations, viz.,

$$\boldsymbol{V}\cdot\boldsymbol{n} = 0 \quad (2)$$

where $\boldsymbol{n}$ is the outward unit vector normal to the surface, and $\boldsymbol{V}$ is the local flow velocity vector.

Trailing-edge vortex sheet: This sheet was assumed to coincide with the two grid surfaces emanating from the blade's trailing edge. Continuity of the normal velocities across the wake cut was enforced through the condition

$$\phi_{\zeta\zeta} = 0$$

On the vortex sheet, the vorticity transport equation was solved, i.e.,

$$\Gamma_\tau + U\Gamma_\xi = 0$$

these two conditions were sufficient to solve for the velocity potential function at the two node points located on either side of the vortex sheet.

Modeling of far-wake effects: To complete the numerical boundary value problem for the physical flow we must also account for the blade tip vortices, the remainder of the wake system that lies outside the computational region, and any wake elements that might have passed out of and returned into the computational region. As mentioned earlier, the near wake is accounted for in the potential solution through the jump in the velocity potential at the blade's trailing edge. The influence of the far wake, as well as the influence of the re-entering wake elements, were modeled in the form of a spanwise variation of an induced flow (or equivalently an induced angle of attack) at the quarter-chord line of the blade. These angles were provided through a separate computation using the free-wake model in the comprehensive rotor trim code CAMRAD/JA.[14] Once the inflow angles were calculated at the computational stations through spanwise interpolations, the angles were then converted into surface transpiration velocities that were implicitly represented in the velocity $\boldsymbol{V}$ in Eq. (2).

Modified Garabedian–McFadden Inverse Design Method[12]

The small disturbance theory for the linearized two-dimensional subsonic and supersonic flows past a wave-shaped wall[13] form the basis of this method. For supersonic flow, the surface pressure can be expressed as

$$C_p = (2/\sqrt{M_\infty^2 - 1})z_x$$

for subsonic flow as

$$C_p = [2/(\pi\sqrt{1 - M_\infty^2})]z_{xx}$$

The previous expressions illustrate the dependence of the local pressure C_p on the freestream Mach number M_∞, and the local slope z_x and curvature z_{xx} of the surface. By combining these expressions, Malone et al.[16] have demonstrated that a more general equation that relates the changes in the surface pressures to the changes in the normal surface ordinates Δz, viz.,

$$A\Delta z + B\Delta z_x + C\Delta z_{xx} = p_c - p_t \tag{3}$$

can be used in the design of airfoil sections. In Eq. (3), A, B, and C are arbitrary constants that determine the convergence rate for the solution, and p_c and p_t are, respectively, the RFS2-computed and user-prescribed target surface pressures at the selected radial control stations.

Equation (3) is discretized using first-order accurate upwind differencing (in the streamwise direction) for the first derivative and second-order accurate central differencing for the second derivative. In difference form, Eq. (3) can be written as

$$L_i\Delta z(i - 1) + D_i\Delta z(i) + U_i\Delta z(i + 1) = R_i \tag{4}$$

where L_i, D_i, U_i, and R_i are coefficients given by the following:

For the upper surface of the airfoil:

$$L_i = -C/\{[(x(i) - x(i - 1)][x(i + 1) - x(i)]\}$$

$$U_i = B/[x(i + 1) - x(i)] + L_i$$

$$D_i = A - L_i - U_i$$

$$R_i = p_c(i) - p_t(i)$$

For the lower surface of the airfoil:

$$U_i = -C/\{[(x(i) - x(i - 1)][x(i + 1) - x(i)]\}$$

$$L_i = B/[x(i + 1) - x(i)] + U_i$$

$$D_i = A - L_i - U_i$$

$$R_i = p_t(i) - p_c(i)$$

Equation (4) is then applied in a streamwise marching fashion (i.e., starting from the leading edge and moving toward the trailing edge) to each of the grid nodes on the upper and lower surfaces of the airfoils at the a priori defined radial control stations. In this study, four radial stations were selected (see Fig. 2). These stations were positioned at the nondimensional radial positions of 0.65, 0.80, 0.93, and 1.0. At each control station, the application of Eq. (4) resulted in two tridiagonal systems of equations that were solved using the Thomas algorithm to determine the changes in the normal ordinates Δz of the airfoil. Our experience has indicated that approximately 15–20 iterations were required to meet a tolerance of 0.001 in the difference between p_c and p_t. The application of Eq. (4) was repeated again at the remaining radial control stations to yield new definitions of the airfoil geometries that constitute the blade. At the computational stations that did not coincide with any of the four control radial stations, the airfoil geometries were linearly interpolated using the definitions of the neighboring airfoil geometries at the nearest control stations and/or the geometry of the baseline NACA-0012 airfoil. Once the geometric definition of the blade was completed, a new three-dimensional computational C–H grid was generated in preparation for the next solution using the RFS2 three-dimensional rotor flow solver. A flow chart depicting these steps is given in Fig. 3.

At this juncture, it is noteworthy to mention that the inverse procedure adopted in this study is more suitable than others since it preserves the chord length of the original airfoil, and hence, the original blade solidity. For example, in hodograph-based design methods[4,7] closure of the trailing edge of the resulting airfoil is not enforced. The final airfoil geometry is usually obtained by altering the target pressure distribution in the vicinity of the leading and trailing edges to minimize the size of the trailing-edge gap and/or to eliminate any upper and lower surface crossings that could result in an airfoil having a fish tail. In these methods, however, because the solution to the inverse problem is treated as one for a free surface, changes in both coordinate directions (i.e., Δx, Δz) are therefore allowed. As a result, it is quite difficult to maintain the chord length of the original airfoil unless scaling of the coordinates of the designed airfoil are made. In the present method, two anchor points, namely, the leading- and trailing-edge points, are used to fix the pressures as well as the chord length of the original airfoil. Moreover, their relative positions also fix the angle of attack of the section. Changes to the airfoil section geometry are thus achieved through changes in the z-coordinate direction, which primarily influence the thickness distribution, and hence, the camber.

Lifting-Line CAMRAD/JA Trim Model

As mentioned earlier, the present design procedure utilizes the lifting-line helicopter/rotor trim code CAMRAD/JA[14] to introduce the rotor trim constraints and the far-wake effects into the RFS2 three-dimensional rotor flow solver. This pro-

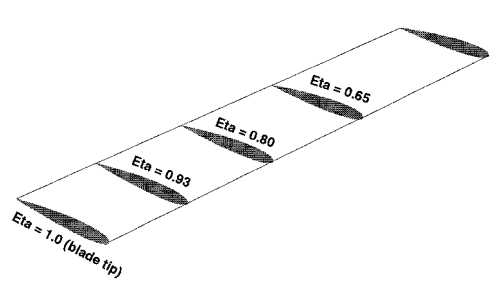

Fig. 2 Sketch depicting the nondimensional radial positions (*Eta = R/Rtip*) for the four control stations selected in this study.

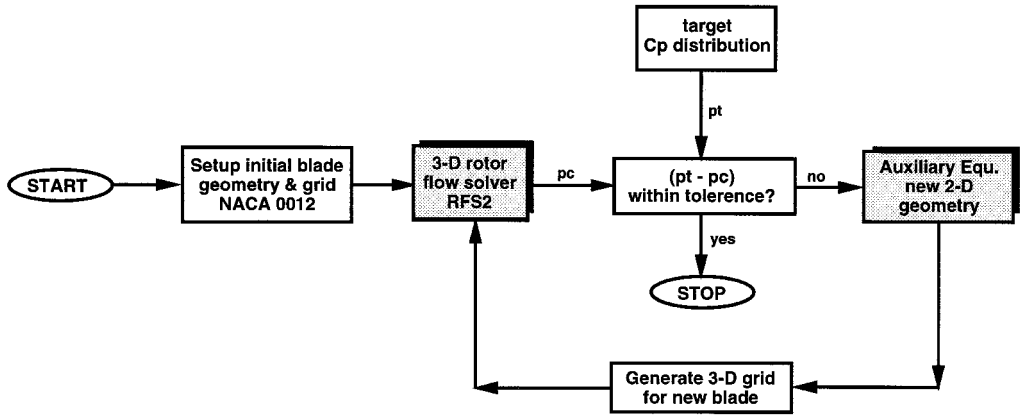

Fig. 3 Flow chart depicting the three-dimensional aerodynamic design procedure for a given pressure distribution.

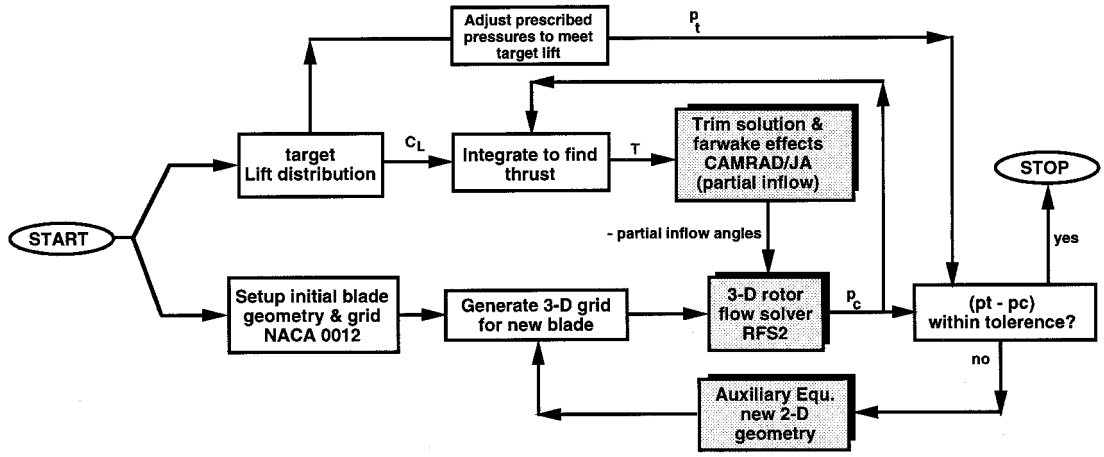

Fig. 4 Flow chart depicting the three-dimensional aerodynamic design procedure for a given lift distribution including the effects of the far wake.

cess is very similar to the traditional CAMRAD/JA-CFD coupled lift solutions described in the literature.[17,18] In this study, however, the desired lift distribution, and hence, rotor thrust, are known a priori and remain fixed throughout the iterative process. For example, after each CAMRAD/JA solution, instead of using RFS2 to recompute the lift distribution based on the CAMRAD/JA-predicted far-wake inflow, differences in lift coefficients based on the target and the current CAMRAD/JA values are used to initiate the subsequent CAMRAD/JA solution. In this respect, the CAMRAD/JA trim solution approaches the target lift distribution, and hence, the target thrust. The result of this iterative process is, of course, far-wake partial angles of attack that are now consistent with the specified target lift distribution. These angles are then used in the subsequent predictions using the two-dimensional inverse solver and the RFS2 full potential rotor flow solver to account for the far-wake-induced effects. A flow chart depicting these steps is shown in Fig. 4.

The initial CAMRAD/JA trim solution is obtained using a starting blade geometry, which consists of a given planform, twist, and airfoils for which C-81 data tables containing the sectional lift, drag, and moment characteristics are available. Here, the starting blade geometry is that of a rectangular blade that has NACA 0012 airfoil sections. The initial CAMRAD/JA trim solution provides a lift distribution that is consistent with this starting geometry, but not necessarily with the target lift distribution. In subsequent iterations, the blade planform is not changed, and hence, the blade geometric solidity. The target lift distribution that is repeatedly used in the subsequent CAMRAD/JA trim solutions may be viewed as an externally generated CFD-based solution that reflects the changes in the airfoil geometries at the four control radial stations. The differences in the lift coefficients (between those computed using CAMRAD/JA and those of the target distribution) are then considered corrections to the CAMRAD/JA airfoil table values because of the corresponding changes in the airfoil geometries.

Results and Discussion

In this section two examples that delineate the use of the present design procedure are given. In the first example, the flexibility of the design method is demonstrated through three exercises that illustrate how one can change the local aerodynamic characteristics/features (sectional lift, strength, and position of the shock wave, and sectional moment) of a given section while maintaining the original local onset flow conditions (i.e., Mach number and angle of attack). For this example, a simple untwisted rectangular blade having an aspect ratio of 12 (6-ft radius, 6-in. chord) and the NACA 0012 airfoil for the various sections along its length is used as the starting (or initial) blade. Far-wake effects were not included in this example. In the second example, the same baseline blade with 9 deg of linear twist is used. The redesign of the blade to meet a target lift distribution with the inclusion of the far-wake effects is presented.

Example 1: Redesign of an Untwisted Blade for a Given Pressure Distribution—No Far-Wake Effects Included

In this example, the goal is to find the airfoil geometries that meet certain target aerodynamic characteristics and/or features at three radial control stations. Figure 5 depicts the initial and the final pressure distributions at three radial stations located at *Eta* = *R*/*Rtip* = 0.65, 0.80, and 1.0. Here, the initial pressure

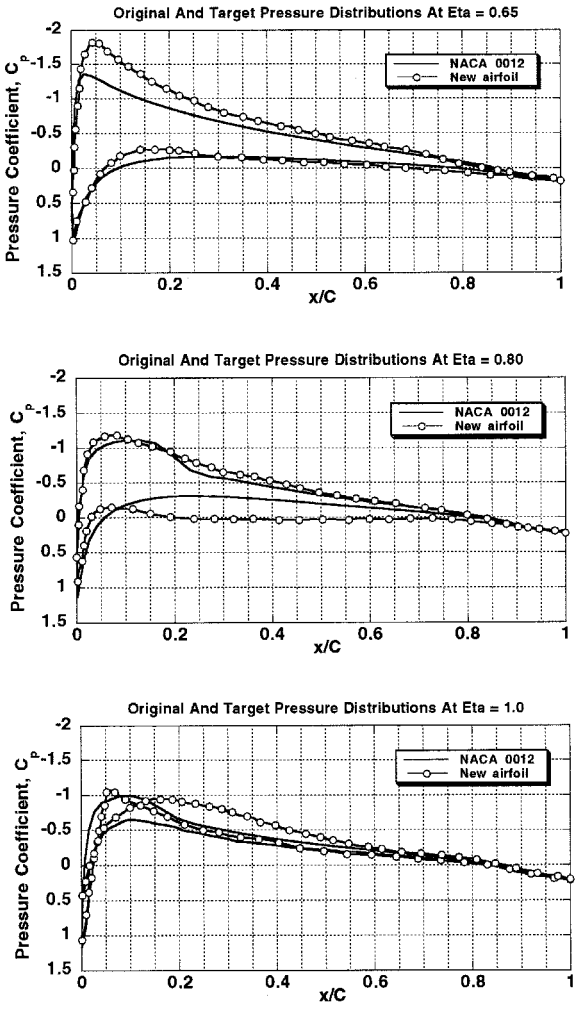

Fig. 5 Starting and final surface pressures for the newly designed blade at three user-specified control stations (*Mtip* = 0.75, no twist, no far-wake effects).

distributions were computed for the baseline blade using the three-dimensional, full-potential rotor flow solver RFS2. The final pressure distributions are those computed using the RFS2 flow solver with the new definition of the airfoil geometries at all four radial control stations. Starting pressure distributions for the RFS2 flow solver were generated by setting the blade at a uniform angle of attack of 4 deg (equivalent to a 4-deg collective pitch). The blade rotational tip Mach number was equal to 0.75 to give rise to a pocket of supercritical flow on the surface of the blade near the tip.

At *Eta* = 0.65 the main objective was to increase the sectional lift value of the original NACA 0012 section while maintaining smooth pressure gradients and, of course, the original onset flow conditions. With the increase in sectional lift a corresponding increase in the sectional drag force should also be expected. An improvement in rotor performance, and in particular, power requirement, would result if this increase in drag is accompanied simultaneously by a more inboard shift in the radial position of the section. This point is addressed in more detail in Example 2.

At *Eta* = 0.80, the objective was to smear the weak shock wave that was present near the 25% chord position. The NACA 0012 airfoil section had a supercritical flow region that extended between the 2–25% chordwise positions. As seen in Fig. 5, for the redesigned section, this region has been slightly extended to the 28% chord position, yet with a smooth shock-free transition to subsonic flow. It is therefore of utmost importance that one start with a target pressure that is shock free or, at least, a distribution that reflects the presence of a very weak shock. In certain instances, which depend largely on the onset flow conditions, one might also be able to find an airfoil geometry that results in a purely subcritical pressure distribution. However, if this pressure distribution is not physically attainable, then the inverse calculations eventually diverge and no airfoil geometry is found.

At *Eta* = 1.0, though theoretically the sectional lift should drop to zero, the predicted value using RFS2 was equal to 0.051. At this section, the target pressure distribution resulted in a sectional lift value of −0.063. The target pressure, however, was selected primarily with the objective of significantly changing the sectional moment characteristics. For the baseline section, a positive moment (i.e., nose up) was obtained. For the redesigned section, a small, but negative (i.e., nose down), sectional moment was obtained. This was achieved by prescribing a pressure distribution that reflects negative loading on portions of the section (i.e., by selecting pressures that have lower values on the lower surface than the values on the upper surface). In this example, note that crossings of the upper and lower surface pressures occur at two chordwise positions, namely, 0.045 and 0.125. Note also that one could have selected a pressure distribution that yields one, rather than two, intersection points between the upper and lower surface pressure distributions. This, of course, would have resulted in a different airfoil geometry.

To determine the overall lift capability of the blade, integration of the predicted sectional lift values at the 18 radial computational stations was performed. To account for the radial variation in the dynamic pressures, the integration was performed for the product of the sectional lift values times the square of the radial position.

Blade lift capability:

$$\alpha \int_{R1}^{R2} r^2 \cdot C_L(r) \cdot \mathrm{d}r \tag{5}$$

where $R1$ is the nondimensional radial position for the innermost computational station (located at 0.55), $R2$ is the nondimensional radial station corresponding to the last computational station on the surface of the blade (i.e., $R2 = 1$), and $C_L(r)$ is the local integrated sectional lift value at a given radial station r. For the baseline and redesigned blades, the application of Eq. (5) resulted in values of 0.0272 and 0.0349, respectively. For a given tip speed, this change represents an increase of 28.3% in the lift capability of the original blade. Figure 6 depicts the original (NACA 0012) and the redesigned airfoil sections that result in the chordwise pressure distributions shown in Fig. 5.

Example 2: Redesign of a Twisted Blade for a Given Lift Distribution — Far-Wake Effects Included

In this example, the baseline blade has a rectangular planform and is again constructed using the NACA 0012 airfoil. With the exception of 9 deg of built-in twist (linearly varying), the blade is identical to the baseline blade described in Example 1. It is our goal here to redesign this blade such that the original lift capability is unchanged. Though this problem may not be of practical interest, it demonstrates how the aerodynamic design engineer can alter the radial variation of the lift distribution which, in turn, influences the overall performance of the hovering rotor caused primarily by the changes in airfoil drag, and hence, rotor power.

Unlike the previous example, where the goal was to match a number of target pressure distributions, here our goal is to match a number of target lift distributions at a given number of radial stations. To reduce the CPU time requirements for the iterative process in the modified Garabedian–McFadden design procedure,[12] we start by prescribing pressure distributions that are uniformly scaled on the upper and/or the lower

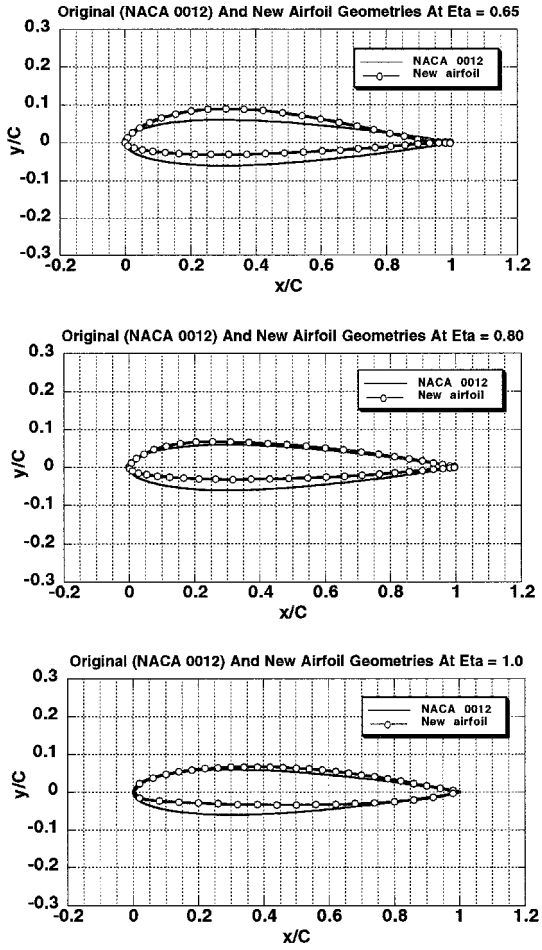

Fig. 6 Initial and final airfoil geometries at three user-specified control stations (*Mtip* = 0.75, no twist, wake effects not included).

surfaces to match the target lifts. That is, given a starting target lift, one selects a pressure distribution that is typically smooth and is free from strong chordwise gradients that can potentially induce the separation of the boundary layer. For supercritical flows, one can start with a pressure distribution that reflects the presence of a smeared (i.e., weak) shock. One can also increase the chordwise extent of the supercritical flow region and transition to subsonic flow through a weak shock in lieu of a more compact region that is terminated with a stronger shock. In the first iteration of the inverse method, integration of this pressure distribution will not necessarily result in a sectional lift value that matches the target lift at this station. Prior to the next iteration, one adjusts the upper and/or lower surface pressure levels, not through varying the individual chordwise pressure values, but through the multiplication of all chordwise values by a constant F, which can be larger or less than 1 to, respectively, increase or decrease, the sectional lift values.

As mentioned earlier, during this iterative process the pressure values at the leading and the trailing edges of the airfoil are held fixed. Typically, this iterative procedure for computing the correct multiplicative factor to achieve the target lift converges in about 4–5 iterations using a Newton-type iteration, viz.,

$$C_L^{m+1} = C_L^m + \frac{\partial C_L}{\partial F}(F^{m+1} - F^m)$$

here the superscripts m, $(m + 1)$ refer to two consecutive iterations and F is the multiplying factor for the upper and/or lower surface pressure distributions.

To predict the aerodynamic performance of the rotor in hover, the prescribed wake model option inherent in CAMRAD/JA[14] was used. In this example, the rotor was trimmed to a thrust level of 0.0751 (C_t/sigma = rotor thrust coefficient/rotor solidity), which resulted in the starting value of 10.01 deg of collective pitch at a rotational Mach number of 0.68. Figure 7 depicts the CAMRAD/JA-predicted sectional lift coefficients (starting or initial values) for the baseline hovering rotor. Also shown are the target sectional lift values that are expected from the redesigned blade. As seen, the target distribution reflects a more gradual radial variation in the sectional lift values as we approach the tip of the blade. This variation necessitated the increases in the sectional lift values between the 0.55 and the 0.865 radial stations and the decrease of the sectional lift values beyond the 0.865 radial station. Note that the sectional lift values inboard of the 0.55 radial station were maintained at the original CAMRAD/JA predicted values.

The CAMRAD/JA code is then used in an iterative process to drive the starting sectional lift values toward the target values while maintaining the thrust level at 0.0751. This process required about 10 iterations. Once a converged solution was obtained, the prescribed wake geometry and the computed far-wake inflow were now consistent with the more favorable target lift distribution. Figure 8 depicts the variation of the CAMRAD/JA-predicted sectional lift values as a function of iteration number. In Fig. 9 we illustrate the variation of the collective pitch angle and the changes in the rotor total power requirement as a function of iteration number. Note that the more uniform target lift distribution results in a 6.5% reduction in the total power. Note also that for the target lift distribution, the required collective pitch angle is 9.45 deg as compared to 10.01 deg for the baseline rotor.

We now take advantage of the fact that the wake geometries, and hence, the wake-induced velocities, are identical for two

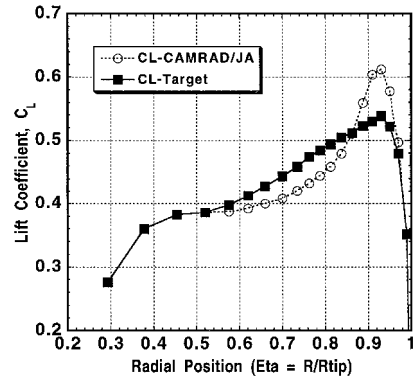

Fig. 7 CAMRAD/JA predicted (initial) and target (final) sectional lift values for the hovering rotor (*Mtip* = 0.68, 9 deg of linear twist).

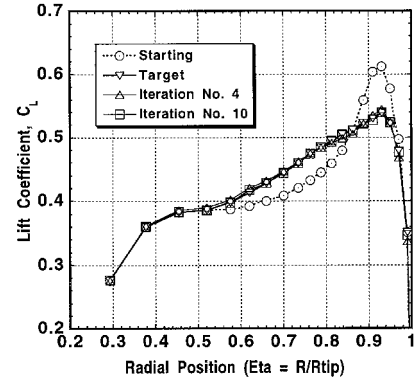

Fig. 8 CAMRAD/JA predicted sectional lift values for various trim iterations (*Mtip* = 0.68, 9 deg of linear twist).

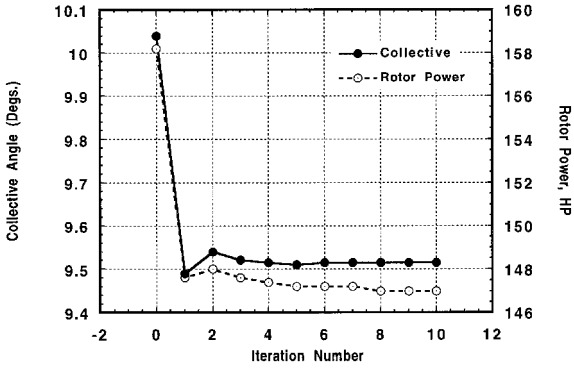

Fig. 9 CAMRAD/JA predicted collective pitch angles and rotor power requirements for various trim iterations (*Ct/S* = 0.0751, *Mtip* = 0.68, 9 deg of linear twist).

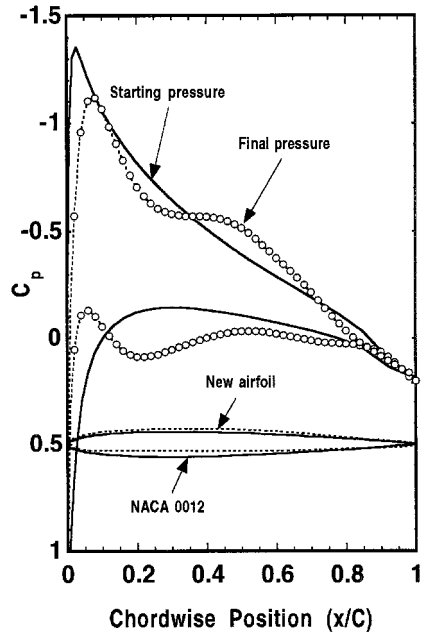

Fig. 10 Predicted surface pressures for the starting and final blade geometries at *Eta* = 0.65 (*Mtip* = 0.68, far-wake effects included, *CL* (starting) = 0.430, *CL* (final) = 0.442).

different blades having the same radial lift distributions. Having computed the far-wake-induced effects that are compatible with the target lift distribution, we begin the coupled two-dimensional inverse/three-dimensional direct solution procedure to search for the new airfoil geometries that meet the target sectional lift values at the four radial control stations along the blade. Note that the control station located at *Eta* = 0.93 was intentionally selected to coincide with the radial position that corresponds to the peak target lift value. For the new airfoils, the resulting thickness ratios will depend primarily on the chordwise variation of the prescribed pressure distributions, the local rotation Mach number, and angle of attack. Therefore, for the new blade, the percent reduction (or increase) in power will depend primarily on the sectional drag characteristics of the new airfoils that constitute the blade. Fortunately, one can infer the expected viscous behavior of the sections by considering certain aspects of the inviscid pressure distributions (e.g., weak shocks, moderate pressure gradients, chordwise position of the peak pressures, etc.).

Figures 10–12 depict comparisons between the predicted starting pressure distributions for the baseline rotor (employing NACA 0012 airfoils) and those predicted for the new blade design at *Eta* = 0.65, 0.80, and 0.93. Also shown in the figures are the starting and final airfoil geometries at these three con-

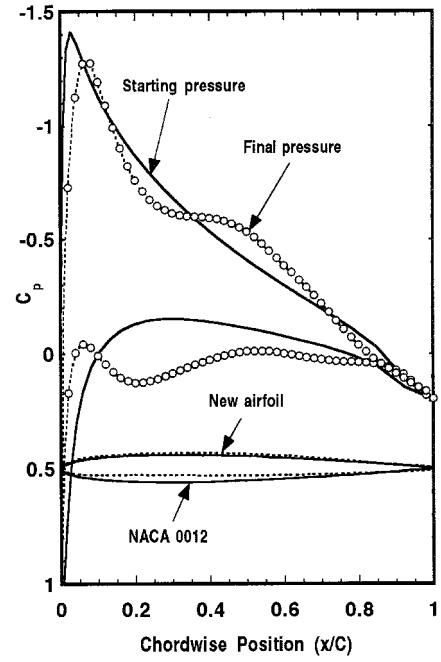

Fig. 11 Predicted surface pressures for the starting and final blade geometries at *Eta* = 0.80 (*Mtip* = 0.68, far-wake effects included, *CL* (starting) = 0.502, *CL* (final) = 0.517).

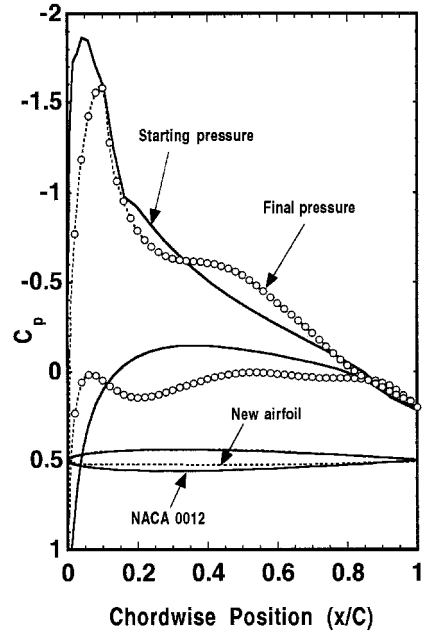

Fig. 12 Predicted surface pressures for the starting and final blade geometries at *Eta* = 0.93 (*Mtip* = 0.68, far-wake effects included, *CL* (starting) = 0.541, *CL* (final) = 0.543).

trol stations. The resulting thickness ratios for the three airfoils are 10.67% at *Eta* = 0.65, 9.81% at *Eta* = 0.80, and 8.8% at *Eta* = 0.93. In prescribing the final pressure distributions our goal was to reduce the magnitude of the suction pressure peaks, increase the chordwise position for the suction peaks, reduce the strength of any existing shock waves, reduce the chordwise extent of the supercritical flow region, and increase the loading on the lower surface to compensate for any loss in lift that may have resulted from reducing the size of the supercritical flow pocket. In Fig. 12, note that the size of the supercritical flow region is significantly reduced. For the NACA 0012 airfoil this region had a chordwise extent equal to 0.15*C*. For the new airfoil, the chordwise extent of the su-

percritical flow region is about 0.06C. As a result, the original strong shock wave associated with the NACA 0012 airfoil was completely eliminated.

To assess the aerodynamic performance characteristics of the new blade design, one can either use the lifting-line CAMRAD/JA code or an alternative, more comprehensive, analysis method that does not require the generation of tables that contain the aerodynamic characteristics of the various airfoil sections. In this study, the latter approach was adopted. Specifically, the aerodynamic performance characteristics of the baseline and the new rotor blades were predicted using the three-dimensional laminar/turbulent thin-layer Navier–Stokes flow solver TURNS.[19] The TURNS flow solver was selected among a few others because of its relative accuracy ($\pm 3\%$) in the prediction of rotor performance.

To predict the aerodynamic performance characteristics of the baseline and redesigned rotors (assumed here to have four blades), two body-fitted computational C–H grids were generated using a hyperbolic grid generator.[20] For the redesigned blade, all radial stations inboard of $Eta = 0.65$ were assumed to have the same airfoil geometry as that at $Eta = 0.65$. For radial stations outboard of $Eta = 0.65$, linear interpolation between the airfoil geometries defined at $Eta = 0.65$, 0.80, 0.93, and 1.0 was used to define the airfoil geometries at the intermediate computational stations. The blade collective angle (9.45 deg) and linear twist (9 deg) were modeled through angular rotations of the grid about the quarter-chord points at the various computational radial stations. The grids had a resolution of 181 nodes in the wraparound C direction (with 144 points on the surface of the airfoil at a given radial station), 49 radial stations (with 30 stations lying on the surface of the blade), and 49 grid points in the direction normal to the surface of the blade. The normal spacing between the first grid points off the surface of the blade and those on the surface was set equal to 0.00005C. The grid was also clustered in the normal direction to adequately resolve the flow in the boundary layer. Approximately 12 grid points were placed in the boundary layer to yield a y^+ value that is on the order of unity.

Inputs to the flow solver included the hover tip Mach number of 0.68 and a Reynolds number (based on a 6-in. chord) of 2.42×10^6. All computations were performed assuming that the flow is fully turbulent in the vicinity of the blade and laminar in the far field. The Baldwin–Lomax turbulence model was used to provide numerical values for the turbulent eddy viscosity. Convergence of the numerical solutions was achieved in approximately 1400 iterations during which the maximum residual fell to a value of 0.2×10^{-6}. On an HP 9000/735 high-performance workstation, the required CPU time was approximately 16.5 h/run.

For the baseline rotor, integration of the sectional lift and drag forces between $Eta = 0.20$ and the blade tip yielded a thrust coefficient C_T equal to 0.008293 and a power coefficient C_P equal to 0.0007379. For the redesigned blade, C_T was equal to 0.0095968 and C_P was equal to 0.0008601. Note that the increase in C_P for the redesigned blade is primarily because of the use of the new airfoil geometry defined at $Eta = 0.65$ for all radial stations inboard of $Eta = 0.65$. At these stations, the predicted sectional lift values are higher than those predicted for the baseline rotor, but the sectional drag values are also higher than those for the baseline rotor. Overall, the lift-to-drag ratio for these airfoils are higher than those for the baseline rotor. To circumvent this problem, additional control stations may be required, say at $Eta = 0.30$ and 0.50 to compute the correct airfoil geometries using the present inverse procedure. Perhaps a more fair comparison of performance would be one where the C_P values are compared for identical thrust coefficients. Substituting the predicted values of C_T and C_P in the expression used to compute the hover figure of merit, viz.,

$$\text{FOM} = (1/\sqrt{2})(C_T^{3/2}/C_P)$$

one obtains a value of 0.7237 for the baseline rotor (using the NACA 0012 airfoils) and a value of 0.7729 for the redesigned rotor (using the new airfoil designs). This represents a 6.36% improvement in the performance of the baseline rotor. In this example, we have demonstrated that through careful selection of the positions of the radial control stations and the starting pressure distributions for the inverse procedure one can design new airfoil sections that can result in the improvement of the performance of the original blade. It is important to stress here, however, that the airfoil geometries found in this example do not, by any means, represent the airfoil geometries necessary to yield the optimum performance by the redesigned blade. Only through trial and error, or through the coupling with an optimization module, can this formidable task be achieved.

Concluding Remarks

A new method for the design of helicopter rotor blade airfoils with allowance for three-dimensional flow effects has been developed. The method is based on the coupled finite difference solutions from two solvers: 1) an efficient two-dimensional inverse solver and 2) a three-dimensional direct full potential flow solver. Based on the results presented, the following conclusions are made:

1) The present inverse design method, in its present form, has some limitations. Most notably in its inability (typical of all inverse methods) to enforce geometric constraints related to the maximum thickness of the resulting airfoil sections. This shortcoming can be overcome using a hybrid method that requires the specification of a portion of the airfoil geometry and the pressure distribution on the remainder of the geometry.

2) Unlike traditional airfoil design methods, we have demonstrated here how the effects of the finite aspect ratio blade, the far wake, as well as the effects of blade planform (i.e., sweep and taper) can be taken into account in the prediction of the airfoil geometries.

3) For more accurate representation of the final blade geometry, the number of radial control stations for the design procedure must be increased to more accurately represent the radial variation of the blade lift values.

4) If the present method is to have a real impact on the aerodynamic design of rotor blades, viscous effects must also be included. This can be easily accomplished through the inclusion of an efficient two-dimensional integral boundary-layer formulation into the RFS2 three-dimensional full potential rotor flow solver, or through the use of an efficient rotor Navier–Stokes flow solver, to provide estimates of the local sectional drag values. Airfoil designs that produce a given radial distribution of lift-to-drag ratios can then be obtained.

5) Though the results presented here focused on the design of airfoil sections for the hovering rotor, the present method was recently extended[21] to the design of airfoil sections for the rotor blade in forward flight.

6) In this study it has not been possible to fully couple the CAMRAD/JA trim code with the two-dimensional inverse/three-dimensional direct codes. More work on this avenue could produce considerable savings in compute time and, more importantly, a viable design tool that can result in significant payoffs in design cost and product efficiency.

7) The present design method represents the first step toward bridging the gap between traditional two-dimensional airfoil design methods and the more comprehensive methods that are based on the solutions to the three-dimensional Euler and Navier–Stokes equations.

Acknowledgment

The authors thank L. N. Sankar of the Georgia Institute of Technology for making available the two-dimensional inverse design code developed under U.S. Army Research Office funds.

References

[1]Hicks, R. M., and Vanderplaats, G. N., "Application of Numerical Optimization to the Design of Supercritical Airfoils," Society of Automotive Engineers, Paper 770440, March 1977.

[2]Davis, W. H., "Techniques for Developing Design Tools from the Analysis Methods of Computational Aerodynamics," AIAA Paper 79-1529, July 1979.

[3]Eppler, R., and Sommers, D. M., "A Computer Program for the Design and Analysis of Low Speed Airfoils," NASA TM 80210, Aug. 1980.

[4]Hassan, A. A., Sobieczky, H., and Seebass, A. R., "Shock-Free Transonic Airfoils with a Given Pressure Distribution," *Journal of Computer Methods in Applied Mechanics and Engineering*, Vol. 58, Feb. 1986, pp. 285–304.

[5]Volpe, G., and Melnik, R. E., "The Role of Constraints in the Inverse Design Problem for Transonic Airfoils," AIAA Paper 81-1233, June 1981.

[6]Tranen, T. L., "A Rapid Computer Aided Transonic Airfoil Design Method," AIAA Paper 74-501, June 1974.

[7]Bauer, F., Garabedian, P., and Korn, D., "Supercritical Wing Sections III," *Lecture Notes in Economics and Mathematical Systems*, Springer–Verlag, New York, 1977.

[8]Fung, K. Y., Sobieczky, H., and Seebass, A. R., "Shock-Free Wing Design," *AIAA Journal*, Vol. 18, No. 10, 1980, pp. 1153–1158.

[9]Silva, D. H., and Sankar, L. N., "An Inverse Method for the Design of Transonic Wings," AIAA Paper 92-1025, Feb. 1992.

[10]Sankar, L. N., and Prichard, D., "Solution of Transonic Flow past Rotor Blades Using the Conservative Full Potential Equation," AIAA Paper 85-5012, 1985.

[11]Hazarika, N., "An Efficient Inverse Method for the Design of Blended Wing-Body Configurations," Ph.D. Dissertation, Georgia Inst. of Technology, Atlanta, GA, June 1988.

[12]Garabedian, P., and McFadden, G., "Design of Supercritical Wings," *AIAA Journal*, Vol. 20, No. 3, 1982, pp. 289–291.

[13]John, J. E. A., *Gas Dynamics*, Allyn and Bacon, Boston, 1969.

[14]Johnson, W., "A Comprehensive Analytical Model of Rotorcraft Aerodynamics and Dynamics. Volume I: Theory Manual, Volume II: User's Manual," Johnson Aeronautics, Palo Alto, CA, 1988.

[15]Jameson, A., "Iterative Solutions of Transonic Flow over Airfoils and Wings Including Flows at Mach 1," *Communications on Pure and Applied Mathematics*, Vol. 27, 1974.

[16]Malone, J. B., Vadyak, J., and Sankar, L. N., "Inverse Aerodynamic Design Method for Aircraft Components," *Journal of Aircraft*, Vol. 24, No. 2, 1987, pp. 832–838.

[17]Strawn, R., and Tung, C., "The Prediction of Transonic Loading on Advancing Helicopter Rotors," NASA TM-88238, April 1986.

[18]JanakiRam, R. D., Hassan, A. A., and Agarwal, R., "Rotorcraft Computational Fluid Dynamics — Recent Developments at McDonnell Douglas," 14th European Rotorcraft Forum, Paper 16, Milano, Italy, 1988.

[19]Srinivasan, G. R., and Baeder, J. D., "TURNS — A Free-Wake Euler/Navier-Stokes Numerical Method for Helicopter Rotors," *AIAA Journal*, Vol. 31, No. 5, 1993, pp. 959–961.

[20]Baeder, J. D., and Srinivasan, G. R., "Computational Aeroacoustic Study of Isolated Blade-Vortex Interaction Noise," American Helicopter Society Aeromechanics Specialist Meeting, Washington, DC, Jan. 1994.

[21]Tapia, F., Sankar, L. N., and Schrage, D. P., "An Inverse Aerodynamic Design Method for Rotor Blades in Forward Flight," 51st Annual Forum of the American Helicopter Society, Fort Worth, TX, May 1995.